Published in IET Electric Power Applications
Received on 5th June 2009
Revised on 25th August 2009
doi: 10.1049/iet-epa.2009.0134

ISSN 1751-8660

Analysis of synchronous reluctance machine with magnetically coupled three-phase windings and reactive power compensation

A.S.O. Ogunjuyigbe[1] *A.A. Jimoh*[1] *D.V. Nicolae*[1] *E.S. Obe*[2]

[1]*Department of Electrical Engineering, Tshwane University of Technology, Pretoria, South Africa*
[2]*Department of Electrical Engineering, University of Nigeria, Nsukka, Nigeria*
E-mail: aogunjuyigbe@yahoo.com

Abstract: Synchronous reluctance machine with simple salient rotor is known to have poor power factor because of its poor reactance ratio. This study presents the use of an auxiliary winding attached to a balanced capacitor to improve the effective reactance ratio as well as the performance characteristics of synchronous reluctance machine. A unique feature of this configuration is that although the machine runs at synchronous speed, the effective reactance ratio of the machine can be improved by appropriate sizing of the capacitor attached to the auxiliary winding, with the constraint of the ampere turn rating of the auxiliary winding. The operational characteristics of a simple salient rotor synchronous reluctance machine equipped with this configuration were investigated and shown to have a desirable performance. How the effective reactance ratio, power factor and airgap flux distribution depend on the size of capacitor attached to the auxiliary winding is determined using a simplified mathematical model of the system. Analytical results and experimental measurements are in good agreement, and demonstrate the effectiveness and benefits of the configuration.

1 Introduction

Synchronous reluctance machine is a singly salient machine in which the rotor is constructed to use the principle of reluctance torque to produce electromechanical power. It is one of the oldest types of electric motors, and has since attracted significant research effort of investigators to improve its performance [1–5]. It is now seen as a viable alternative to other AC machines because of its simple rugged rotor structure, relatively inexpensive, comparatively low rotor inertia, high torque density and the absence of rotor windings leading to reduced rotor losses [6–8]. The performance characteristics of this machine have been shown in literature to be dependent on its saliency ratio (X_d/X_q) and the torque index ($X_d - X_q$), thus most of the research efforts were focused to maximising them. Commonly, attempts at maximising these factors have been geometrical based, which has led to the emergence of different rotor structures [3, 9]. A general review of the different rotor configurations has shown that the synchronous reluctance machine with conventional salient-pole rotors has a low power factor and low torque/weight ratios because of low effective reactance ratio (X_d/X_q), therefore it has become unpopular for practical applications. However, the desire to improve its performance characteristics motivated the use of phase number higher than three, and also the addition of a proper level of third harmonic of current to interact with the third harmonic magnetic field in the synchronous reluctance motors [10, 11]. This method summarily gave about 10% torque improvement without any corresponding improvement in power factor, since the power factor depends on the saliency ratio, which to date is known to be dependent on the rotor geometry. Meanwhile the different rotor structures that have been developed suffered one shortcoming or another, ranging from high manufacturing cost, difficulty to manufacture, to their mechanical integrity in high-speed application.

The power factor of a synchronous reluctance can be improved by reactive power compensation through the

installation of capacitor banks; however, these capacitor banks have been found to result in problems particularly when there is a loss of supply [12]. If the capacitors are series connected and external, it will invariably lower the overall impedance of the machine and result in higher current drawn from the supply, which could damage the windings with a negligible improvement in power factor. Also, using a shunt capacitor, on the other hand, improves the power factor of the external supply rather than the inherent power factor of the machine [13]. It was also reported in [13] that the use of either of these methods can cause problems at light load conditions and relatively expensive switchgear are required to vary the capacitance value with load changes. Thus the use of either the external series or the shunt capacitor seems not to present an absolute practical method for the improvement of the power factor.

In the last three decades, two previous capacitor connection schemes invented by Wanlass [14, 15] and Roberts [16] have been applied to induction motors. The first scheme connects capacitors in series with a second winding and connects the same winding and the first to the same supply. Whereas in the second scheme popularly known as the 'unity-plus winding motor', only one winding set is connected to the supply whereas the other winding set is connected to the capacitors only. These schemes are illustrated in Figs. 1*a* and *b* for a delta-connected machine. These two schemes were, respectively, investigated in [16, 17] and it was generally reported that they both offered a lower efficiency than the conventional induction machine. However, the 'unity plus winding motor' claimed a power factor near unity and better efficiency than the Wanlass motor. One common feature of both the Wanlass and Roberts schemes is that both are applied to induction motors. A well-designed induction motor operates above 0.85 power factor and efficiency of about 90%, and hence such a connection scheme is hardly worth it. Despite the similarity in construction of induction and line-start reluctance motors, induction motors develop torque by interaction of airgap field with rotor currents whereas reluctance machine torque is uniquely dependent on the difference between the reactances on the direct and quadrature axis (torque index) in relation to the alignment principle. Whereas the power factor of the induction machine is influenced by the magnetising reactance, that of the reluctance motor is dependent on the ratio of the reactance on the direct to the quadrature axis (effective saliency ratio). For these reasons, the connection scheme that offers a high power factor (which is usually low in reluctance machines) is adopted in this study [18, 19]. It does not require special switchgear for the switching of the capacitor, since a typical capacitance value is found to properly compensate for all loads. This is similar to the configuration applied to induction machine in [12].

As indicated above, while research efforts have been concentrated in maximising the torque index and saliency ratio through geometrical means this paper introduces a

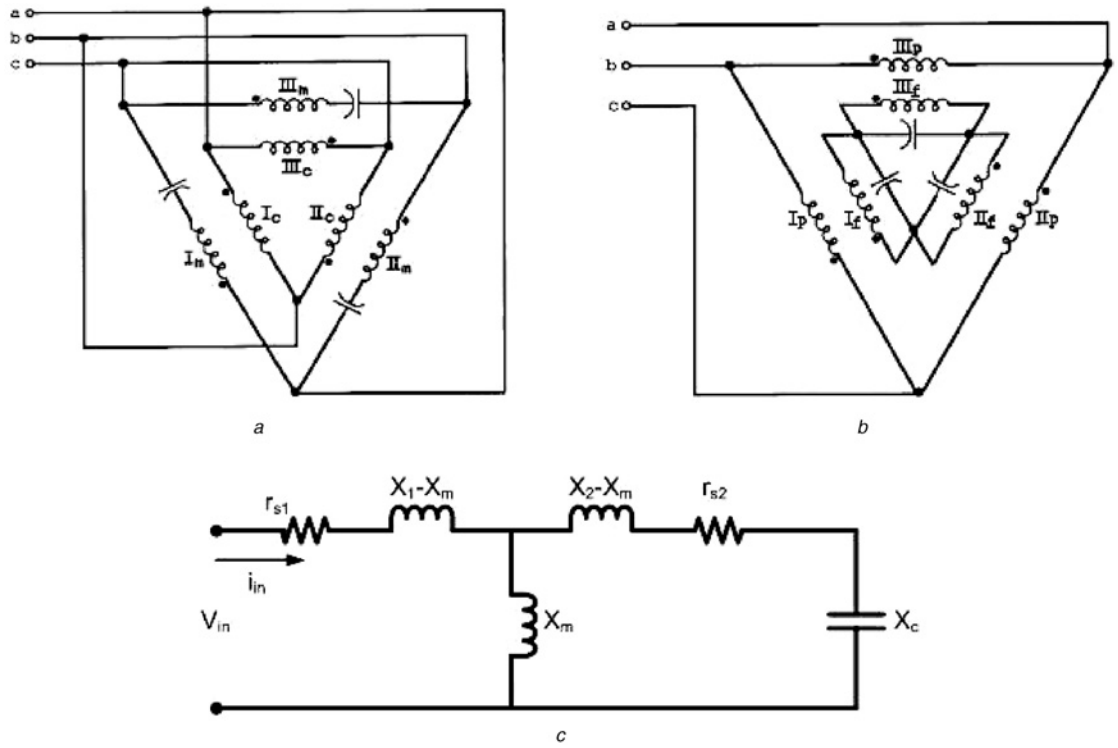

Figure 1 *Connections for capacitance injection*

a Wanlass connection
b Roberts's connection
c Per phase equivalent circuit of a synchronous reluctance machine with dual winding and capacitance injection

IET Electr. Power Appl., 2010, Vol. 4, Iss. 4, pp. 291–303
doi: 10.1049/iet-epa.2009.0134

novel approach of increasing the effective saliency ratio for improved performance characteristics. By way of description, the scheme consists of a stator modified along the split winding concepts to have two symmetric three-phase windings having the same number of poles, and a conventional salient-pole rotor. The two windings occupy the same slot and are magnetically coupled. The first winding identified as the main winding-*abc* is connected directly to utility supply, thus it carries the load current, whereas the second winding- auxiliary-*xyz* is attached to a balanced capacitor for leading current injection, so that the main winding current can be influenced towards leading. The concept of machine having a stator with two similar but separate windings wound for the same number of poles has been used as a means to increase the power capability of large alternators, to overcome the limitation imposed by the fault current interrupting capacity of circuit breakers [20, 21], and to permit electrical segregation of bus sections in large stations [22]. Drives based on these winding arrangements have improved torque and magnetomotive force (MMF) characteristics. The dual stator winding reluctance machine with auxiliary winding connected to a balanced capacitor is considered a promising configuration in view of the absence of copper loss and relatively low core loss on the rotor, and the better performance characteristics obtainable when compared to an equivalent conventional synchronous reluctance machine. With an appropriate size of capacitor attached to the auxiliary winding, the motor operates with an attractive power factor. Outside the cost of the additional winding and capacitor, this configuration presents itself as an attractive and suitable choice because it may on the overall lower the inverter rating of the converter fed reluctance machine as a result of the better power factor that is achievable [23] without modifying the rotor geometry. This paper therefore sets forth an analysis as well as the experimental validation of the operations and benefits of a *p*-pole synchronous reluctance machine with double stator winding and a simple salient rotor.

The remaining part of this paper is organised as follows. Section 2 utilises the coupled circuit analysis to investigate the effect of the capacitance compensation through an auxiliary winding on the effective reactance ratio and the power factor performance characteristics of synchronous reluctance machine with simple salient rotor structure. The magnetic field concept is used to describe the airgap torque of the machine and the nature of its airgap flux distribution in Sections 3 and 4, whereas Section 5 gives the analytical and validating experimental results using a practical laboratory motor. The paper is then concluded in Section 6.

2 Capacitance effect on performance characteristics

The two stator winding sets, *abc* and *xyz*, are magnetically coupled and electrically isolated. Therefore the two stator windings are represented as a coupled circuit with two branches representing the two windings, each having separate resistance, and leakage reactance together with a common mutual reactance [18, 19]. The mutual component arose from the fact that the two sets of stator windings occupy the same stator slots. The branch of the coupled circuit representing the auxiliary winding is connected to a capacitor C with a reactance X_c. This machine structure is easily represented by an approximate per phase equivalent circuit shown in Fig. 1*c*.

Since the machine under consideration is of the salient rotor structure type, the effect of the rotor is manifested in the derivable equivalent circuit of Fig. 1*c* based on the fact that the synchronous impedance will vary with the saliency of the rotor of the machine. The synchronous reactance of a reluctance machine is given as [13]

$$X = \frac{1}{2}(X_d + X_q) + \frac{1}{2}(X_d - X_q)\exp(2\delta) \qquad (1)$$

where X_d and X_q are the steady state *d*- and *q*-axis reactance, respectively and δ is the load angle of the machine. The parameters of the experimental machines are listed in Table 1. The coupled circuit of Fig. 1 along with (2) is used to investigate the effect of the magnetically coupled, two stator windings and capacitance injection on the performance characteristics of synchronous reluctance with simple salient rotor.

Table 1 Machine parameters

Parameter	Value
airgap at pole face, g_1	0.25 mm
airgap between poles, g_2	12.0 mm
number of poles	4
stack length, *L*	148.5 mm
number of turns per coil	45
voltage, *V*	150 V
main winding resistance	4.74 Ω
auxiliary winding resistance	14.9 Ω
frequency, *f*	50 Hz
rated main winding current	8.8 A
direct axis reactance, X_d	43.31 Ω
quadrature axis reactance, X_q	12.60 Ω
pole arc/pole pitch ratio	0.5
stator outer diameter	188 mm
stator Inner diameter, *R*	110 mm

2.1 Effective reactance ratio

Based on the per phase equivalent circuit of Fig. 1, the total per phase impedance of the machine $Z_{\mathrm{T-ph}}$ is obtained as

$$Z_{\mathrm{T-ph}} = (r_{s1} + \mathrm{j}X_{L1}) + [\mathrm{j}X_{\mathrm{m}}//(r_{s2} + \mathrm{j}(X_{L2} - X_{\mathrm{c}}))] \quad (2)$$

where X_{L1} and r_{s1}, respectively, represent the leakage inductance and resistance of the main winding, X_{L2} and r_{s2} represent the leakage inductance and resistance of the auxiliary winding and X_{c} is the reactance presented by the capacitor injected into the machine through the auxiliary winding.

To effectively illustrate the effect of capacitance value on the d- and q-axis reactances of the machine, we substitute, $\delta = 0$ (when the rotor is in the direct axis) and $\delta = \pi/2$ (when the rotor is in the quadrature axis) into (2) and obtain the effective d- and q-axis impedances as

$$Z_d = r_{s1} + \mathrm{j}\left(X_{L1} + X_d\left(\frac{r_{s2} + \mathrm{j}(X_{L2} - X_{\mathrm{c}})}{r_{s2} + \mathrm{j}(X_d + X_{L2} - X_{\mathrm{c}})}\right)\right)$$

and (3)

$$Z_q = r_{\mathrm{s1}} + \mathrm{j}\left(X_{L1} + X_q\left(\frac{r_{s2} + \mathrm{j}(X_{L2} - X_{\mathrm{c}})}{r_{s2} + \mathrm{j}(X_q + X_{L2} - X_{\mathrm{c}})}\right)\right)$$

Neglecting resistances, we obtain the effective d- and q-axis reactances X_d' and X_q' of the machine which when plotted against the capacitance yields (Fig. 2). It can be seen from this figure that there are two resonant points, $X_{\mathrm{c1}} = X_d$ and $X_{\mathrm{c2}} = X_q$. The first point $X_{\mathrm{c1}} = X_d$ is useful, since it yields a very high effective reactance ratio of about 170, whereas the point $X_{c2} = X_q$ gave an extremely low reactance ratio, thus, it has no practical value. Although a seemingly super high reactance ratio, although theoretical is obtained, it will be seen in the next section that a correspondingly high torque cannot be realised, but a very substantial improvement in power factor.

2.2 Impact of the scheme on power factor of the machine

The power factor for the synchronous reluctance machine illustrated with the per phase equivalent circuit of Fig. 1 is evaluated using

$$\cos\,\phi = R_{\mathrm{eq}}/\sqrt{R_{\mathrm{eq}}^2 + X_{\mathrm{eq}}^2} \quad (4)$$

where R_{eq} and X_{eq} represent the effective resistance and reactance of the entire circuit of Fig. 1*c* when viewed from the main source. Equation (4) was arranged in a MATLAB environment and the power factor characteristics of the modified machine as calculated in relation to the size of capacitance at different load angle are shown in Fig. 3. It is observed from this figure that unlike the conventional reluctance machine of the same dimensions (with an estimated maximum power factor of 0.56), the machine with the new configuration offered a power factor of as high as 0.9846. This is due to the presence of the auxiliary winding and capacitance connected, which positively influenced the effective reactance of the machine. A three-dimensional (3D) plot illustrating the variation of the main winding current with the load angle and capacitance is also shown in Fig. 4. While the derivable equivalent circuit of Fig. 1 used in this analysis is an approximation, the general trend in the plots of Fig. 3 taken for different load angles are the same, and it showed that, the inherent power factor of the machine increased with an increase in the size of capacitor attached to the auxiliary winding, and the points of high power factor is found to correspond to the points of minimum current in the main winding.

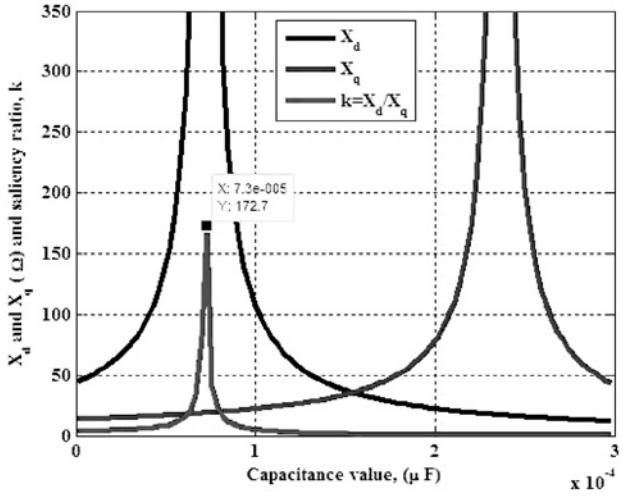

Figure 2 *Effective reactances X_d and X_q and saliency ratio against capacitance*

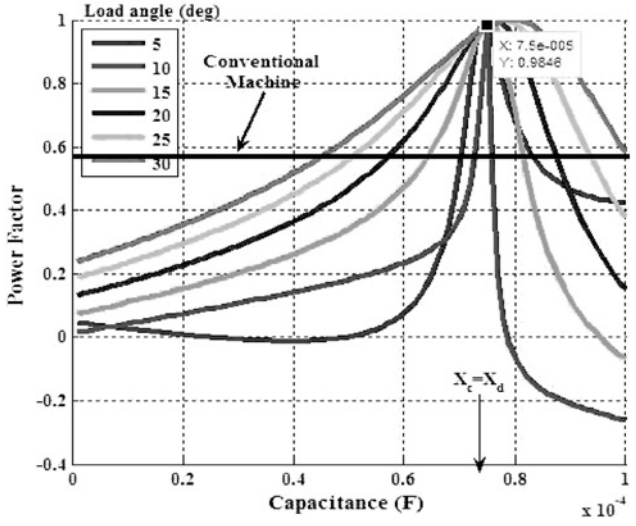

Figure 3 *Plot of power factor against capacitance at different load angles*

IET Electr. Power Appl., 2010, Vol. 4, Iss. 4, pp. 291–303
doi: 10.1049/iet-epa.2009.0134

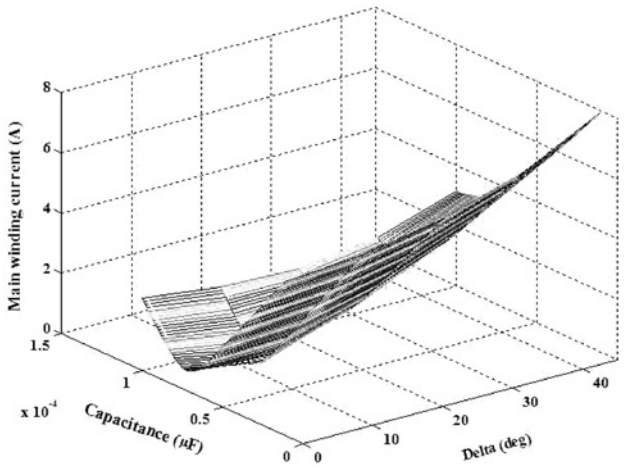

Figure 4 *3D plots showing the variation of the main winding current as a function of load angle and capacitance*

2.3 Selecting the appropriate size of capacitor

In order to determine the capacitance value that will give an improved power factor characteristic, the imaginary part of (2) is set to zero and the equation is solved to determine X_c. It resolves to a quadratic equation having two solutions, as shown in Appendix. The two equations can be plotted for changing δ to give Fig. 5. Although both conditions will naturally give unity power factor, the solution that gives plot with the linear relationship will require capacitance values that will subject the auxiliary winding to high current, so it has no practical value. The other relationship perfectly fits a curve defined by

$$C_{\mathrm{UPF}} = \frac{1}{2}(C_d + C_q) + \frac{1}{2}(C_d - C_q)\cos\ \delta \tag{5}$$

where C_{UPF} is the capacitance that gives a unity power factor,

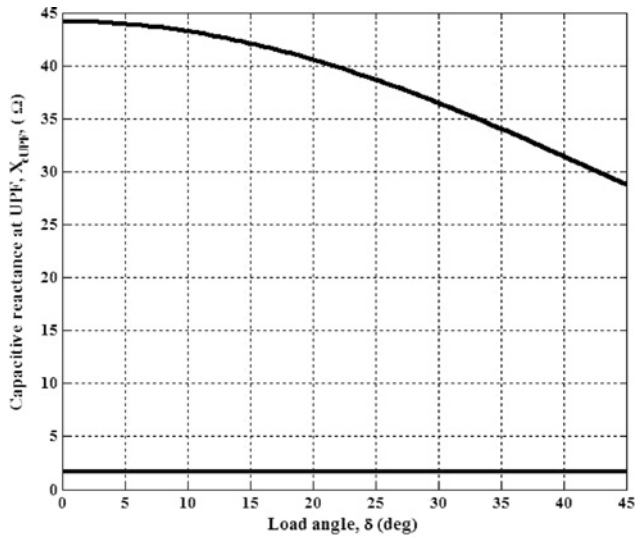

Figure 5 *Variation of capacitance and load angle at unity power factor operation*

C_d and C_q are the capacitance values that will give the $X_c = X_d$ and $X_c = X_q$, respectively. Therefore unity power factor is achievable if the capacitor values can be adjusted to follow the load angle using (5). This capacitor value is, however, subject to the current carrying capability of the auxiliary winding. If $X_c = X_q$, the torque will be very low, because the torque index at this point is very low. On the other hand, if $X_c = X_d$, an optimal effective saliency ratio will be obtained and hence optimal torque and power factor will result.

3 Reluctance motor torque analysis

In this section, the airgap torque of a synchronous reluctance machine with two stator windings and reactive power compensation is presented using the electromagnetic field concepts to determine the flux densities and stored energies, which are then used to determine the electromagnetic torque [18, 24]. Classical assumptions in electrical machine analysis were made to obtain closed form equations [10, 25], thus, only the fundamental components of the stator winding distributions, stator currents and voltages are considered, and the effect of saturation is neglected. These are sufficient enough to explain the fundamental operation of the machine.

If the winding distributions and current of windings *abc* are, respectively, defined as

$$N_k(\theta) = N_{sj}\ \cos\left(p\theta - \varphi_k\right) \tag{6}$$

and

$$I_k(t) = I_{m1}\ \cos\left(\omega t - \alpha_k\right) \tag{7}$$

If $j = 1$, $k = a,\ b,\ c$; $\varphi_a = \varphi_1$; $\varphi_b = \varphi_1 - 2\pi/3$ and $\varphi_c = \varphi_1 - 4\pi/3$, then the parameters refers to the main winding.

The angle θ is the circumferential angle of the stator, whereas N_{s1}, correspond to number of turns per pole per phase for the main winding.

It can then be shown that the resultant MMF because of the winding set *abc* is

$$F_{g1}(\theta, t) = F_{m1}\ \sin\left(\omega t - \alpha + \varphi_1 - p\theta\right) \tag{8}$$

where $F_{m1} = 3/2N_{s1}I_{m1}$ is the peak MMF because of the main winding.

Given that the auxiliary winding *xyz* shares the same magnetic structure and it is magnetically coupled to the main winding *abc*, then, by transformer action, an emf e_{s2}, of similar sinusoidal characteristics as the main source is induced in the auxiliary winding *xyz*. A simplified per

phase representation of the auxiliary winding is shown in Fig. 6.

With a balanced capacitance attached to the auxiliary winding, the emf e_{S2} induced in the auxiliary winding will cause a balanced leading current i_{s2} defined by (9) to flow in the auxiliary windings. The magnitude and phase of this current is largely determined by the impedance of the auxiliary winding *xyz* as influenced by the size of the capacitance attached to the winding *xyz*

$$i_k(t) = I_{m2} \sin(\omega t + \alpha_{ak}) \tag{9}$$

where $k = x,\ y,\ z;\ \alpha_{ax} = \alpha_a;\ \alpha_{ay} = \alpha_a - 2\pi/3;\ \alpha_{az} = \alpha_a - 4\pi/3$ and $\alpha_a = \tan^{-1}(X_2 - X_c/R_2)$.

If the winding distribution of the auxiliary winding *xyz* is given as (6) for the condition $j = 2$, $k = x,\ y,\ z;\ \varphi_x = \varphi_2;\ \varphi_y = \varphi_2 - 2\pi/3$ and $\varphi_z = \varphi_1 - 4\pi/3$, and the winding current as in (9), it can be shown that the MMF because of the leading current flowing in the auxiliary winding *xyz* is

$$F_{g2}(\theta, t) = F_{m2} \sin(\omega t - \alpha_a + \varphi_2 - p\theta) \tag{10}$$

where $F_{m2} = 3/2N_{s2}I_{m2}$ gives the peak value of the airgap MMF because of the auxiliary winding.

Thus, at any arbitrary instant in time, there are two MMF distributions F_{g1} and F_{g2} along the airgap, and the resultant field is sinusoidally time variant and rotating at constant speed ω rad/s. The total airgap MMF $F_{gt}(\theta, t)$ is given as

$$\begin{aligned} F_{gt}(\theta, t) &= F_{g1}(\theta, t) + F_{g2}(\theta, t) \\ &= F_{m1} \sin(\omega t - \alpha + \varphi_1 - p\theta) \\ &\quad + F_{m2} \sin(\omega t - \alpha_a + \varphi_2 - p\theta) \end{aligned} \tag{11}$$

The airgap is not constant because of saliency, but it is a function of the angular position θ and the rotor mechanical angle θ_{rm} and it can be approximated as [10, 13, 24]

$$g^{-1}(\theta, \theta_{rm}) = m + n \cos 2p(\theta - \theta_{rm}) \tag{12}$$

where $m = 1/2(1/g_1 + 1/g_2),\quad n = 1/2(1/g_1 - 1/g_2)$ $\sin(p\tau_p/2),\ \theta_{rm} = \omega t + \delta,\ g_1$ is the airgap at the pole face and g_2 is the airgap between poles.

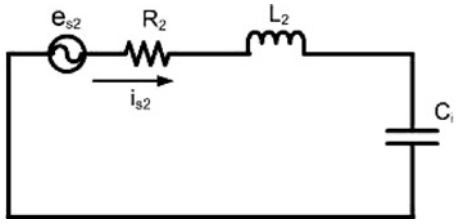

Figure 6 *Per phase representation of the auxiliary winding*

This machine develops torque based on the change of magnetic energy when the rotor moves with respect to the stator MMF pattern. The stored energy E in the magnetic circuit of effective length L is given as

$$E = RL \int_0^{2\pi} \mu_o g^{-1}(\theta, \theta_{rm}) F_{gt}^2(\theta, t) \mathrm{d}\theta \tag{13}$$

When (11) and (12) substituted into (13), is expanded, integrated over the complete circumference, and carefully manipulated using trigonometry identities, some terms becomes zero, leaving terms that are either constant or dependent on the rotor angle δ. Consequently, the energy stored in the magnetic circuit because of the combined airgap MMF of windings *abc* and *xyz* becomes

$$E = RL\mu_o\pi \begin{bmatrix} mF_{m1}^2 - \dfrac{nF_{m1}^2}{2}\cos 2(\alpha - \varphi_1 + \delta) \\ +mF_{m2}^2 - \dfrac{nF_{m2}^2}{2}\cos 2(\alpha_a - \varphi_2 + \delta) \\ -mF_{m1}F_{m2}\cos(\alpha - \alpha_a - \varphi_1 + \varphi_2) \\ -\dfrac{nF_{m1}F_{m2}}{2}\cos(\alpha + \alpha_a - \varphi_1 - \varphi_2 + 2\delta) \end{bmatrix} \tag{14}$$

In (14), only the terms that are dependent on the rotor angular position δ participate in the development of electromagnetic torque. The average electromagnetic torque developed is defined as the rate of change of the stored energy with respect to the rotor angular position, and it is expressed as [24, 26]

$$\begin{aligned} T_{av} &= p_r \frac{\mathrm{d}E}{\mathrm{d}\delta} \\ &= p_r\mu_o\pi RL \begin{bmatrix} F_{m1}^2 \sin 2(\alpha - \varphi_1 + \delta) \\ +F_{m2}^2 \sin 2(\alpha_a - \varphi_2 + \delta) \\ +F_{m1}F_{m2} \sin(\alpha + \alpha_a - \varphi_1 - \varphi_2 + 2\delta) \end{bmatrix} \end{aligned} \tag{15}$$

Equation (15) can be simply expressed as

$$T_{av} = T_{e1} + T_{e2} + T_{e3} \tag{16}$$

It easily follows from (15) and (16) that the torque developed by the machine configuration reported in this paper has three main components identified as T_{e1}, T_{e2} and T_{e3}. The term T_{e1} clearly represents the reluctance torque contribution of the main winding. T_{e2} is similar to T_{e1}, and it is an additional component that represent the unique contribution of the auxiliary winding attached to a balanced capacitance, whereas T_{e3}, the third component of the torque developed by this machine is as a result of the interaction of the two winding currents: main (I_{abc}) and auxiliary (I_{xyz}). The effect of the capacitance on these torque components (T_{e2}, T_{e3}) is manifested in the peak value of the MMF as well as the angle α_{ak} of (9). The second and the third torque components will only be

doi: 10.1049/iet-epa.2009.0134

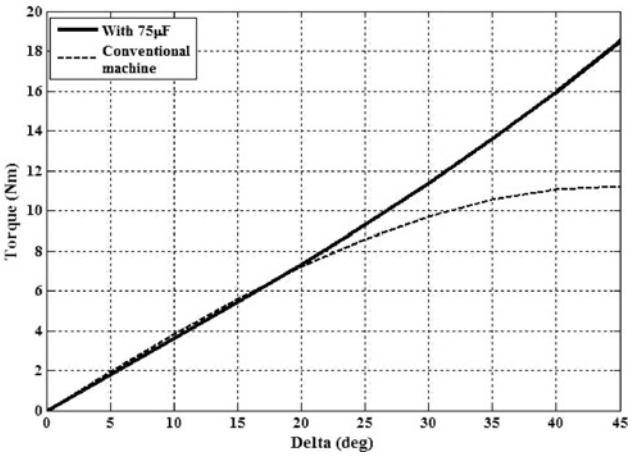

Figure 7 *Improvement in torque against delta at different capacitance*

developed when capacitor is connected to the auxiliary winding. Otherwise T_{e2} and T_{e3} will be set to zero, thus the machine will only act as a standard synchronous reluctance machine. The additional torque components (T_{e2} and T_{e3}) of (16) describe the influence of the magnetically coupled two three-phase windings and reactive power compensation, on the torque performance of the synchronous reluctance machine with simple salient rotor structure. Following the description of Section 2 to make a proper choice of capacitance, the average of the torque component T_{e2} and T_{e3} should be a positive contribution, thus it will make the torque performance to be superior to the standard reluctance machine.

3.1 Impact of the scheme on torque of synchronous reluctance machine

Given the theoretically predicted effective reactance ratio in Section 2.1, and (16) which shows additional torque components, the steady-state electromagnetic torque of the modified machine is here evaluated based on the equivalent circuit of Fig. 1*c*. At steady state, the electromagnetic torque (T_{em}) developed by the modified machine is evaluated using [19]

$$T_{em} = \frac{3V^2 R_{eq}}{(R_{eq}^2 + X_{eq}^2)} \tag{17}$$

The variation of the torque (T_{em}) of the machine fitted with

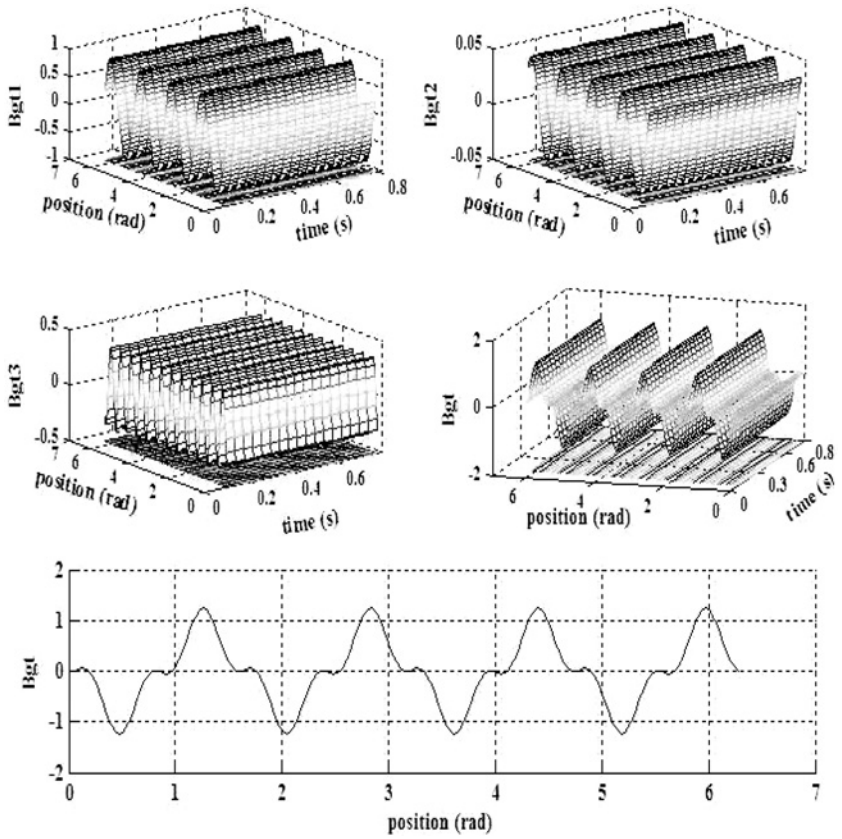

Figure 8 *3D plots of the airgap flux density at $\delta = 25^\circ$ with a capacitance of 5 μF*

a Airgap flux density because of the main winding *'abc'*
b Airgap flux density because of the auxiliary windings *'xyz'*
c Third harmonic content of the airgap flux density
d Total airgap flux density
e Plot of total airgap flux density against position

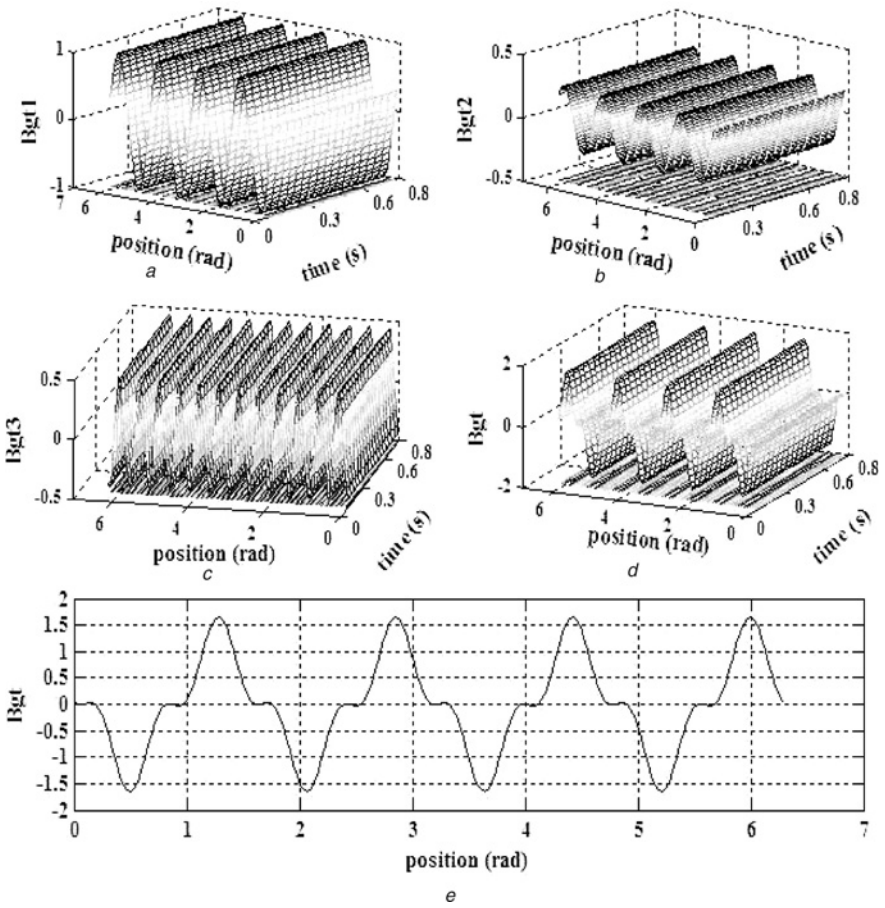

Figure 9 *3D plots of the airgap flux density at $\delta = 25^{\circ}$ with a capacitance of 75 μF*

a Airgap flux density because of the main winding *'abc'*
b Airgap flux density because of the auxiliary windings *'xyz'*
c Third harmonic content of the airgap flux density
d Total airgap flux density
e Plot of Total airgap flux density against position

the configuration is then plotted against the load angle, and compared to that of the conventional reluctance machine in the same curve of Fig. 7.

A relative improvement in torque performance, which is only evident at a load angle of 18° and higher is observed from this figure. This improvement is only possible for a capacitance for which $X_c = X_d$. Furthermore, this improvement is found to increase with an increase in the load angle. At capacitance $X_c = X_q$, a negative torque index is obtained, and the capacitance is too high that it does not represent a practical value. High power factor was correspondingly achieved at the load angles that correspond to the ones where torque improvement is identified.

4 Air-gap flux density

The total airgap flux density at any position along the airgap is defined as

$$B_{gt}(\theta, t) = \mu_o F_{gt}(\theta, t) g^{-1}(\theta, \theta_{rm}) \quad (18)$$

where F_{gt} is the total MMF at any position θ and instant t, derived and expressed by (11), and g^{-1} is the inverse airgap function of a reluctance machine. Substituting (11) and (12) into (18), and simplifying using some trigonometrical

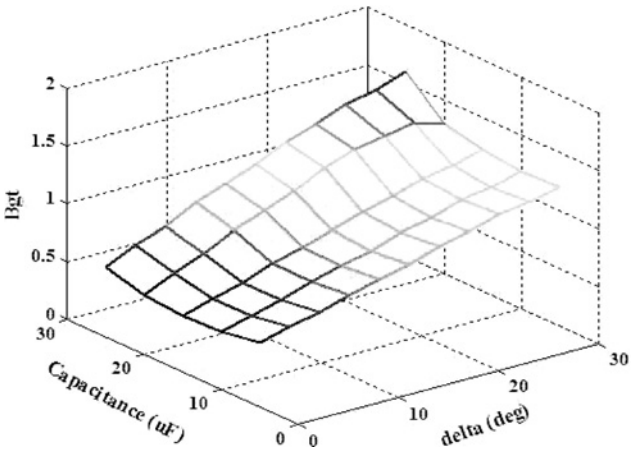

Figure 10 *3D plots of the total airgap flux density as a function of capacitance and delta*

IET Electr. Power Appl., 2010, Vol. 4, Iss. 4, pp. 291–303
doi: 10.1049/iet-epa.2009.0134

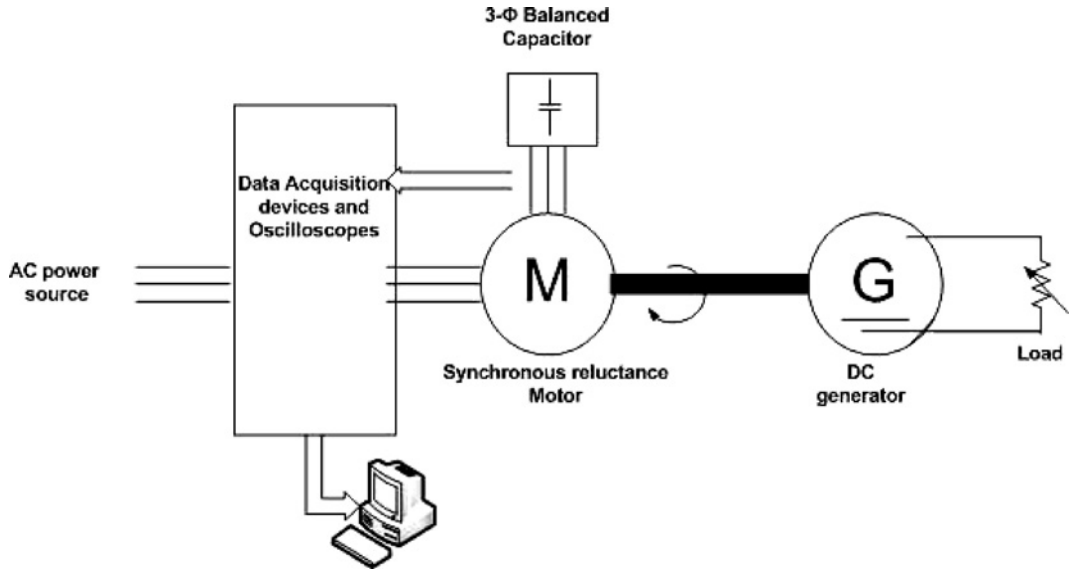

Figure 11 *Experimental set-up*

manipulations, the total airgap flux density becomes

$$B_{gt}(\theta, t) = \begin{bmatrix} B_{m1}\sin(\omega t - \alpha + \varphi_1 - p\theta) \\ +B_{m2}\sin(\omega t - \alpha_a + \varphi_2 - p\theta) \\ +B_{n1}(\sin(p\theta - \omega t - \alpha + \varphi_1 - 2\delta) \\ \quad +\sin(3\omega t - \alpha + \varphi_1 - 3p\theta + 2\delta)) \\ +B_{n1}(\sin(p\theta - \omega t - \alpha_a + \varphi_2 - 2\delta) \\ \quad +\sin(3\omega t - \alpha_a + \varphi_2 - 3p\theta + 2\delta)) \end{bmatrix} \tag{19}$$

where $B_{m1} = \mu_o m F_{m1}$, $B_{m2} = \mu_o m F_{m2}$, $B_{n1} = 1/2\mu_0 n F_{m1}$ and $B_{n1} = 1/2\mu_0 n F_{m2}$

Equation (19) gives the time and space variations of total airgap flux densities produced by the currents in the two windings sets: *abc* and *xyz*. The flux density components B_{m1} and B_{n1} are the peak values of the flux density contributed by the main winding *abc* whereas, B_{m2} and B_{n2} are the peak values of those contributed by the auxiliary winding. The effect of the capacitor on the flux distribution is manifested in the F_{m2} and α_a. These flux components in (19) basically contribute towards the energy conversion.

For the typical experimental machine used in this work, some 3D plots showing the time and space variations of the airgap flux density components produced by the two stator windings when the machine is fitted with a capacitor of 5 and 75 μF at a load angle of $\delta = 25^\circ$ are graphically illustrated in Figs. 8 and 9. These plots and that of Fig. 10 were generated using (19), and the steadystate stator winding currents obtained from experimental measurements on the prototype machine with the parameters specified in Table 1. These figures revealed that the net flux in the stator of the machine with the configuration discussed in this paper is a rotating sine wave. With the different capacitance values considered, the flux density in the airgap maintains the same shape as the standard synchronous reluctance machine, and moves around the inner surface of the stator. In addition, Fig. 10 shows the variation of the airgap flux density as a function of the capacitance injected, and the load angle.

5 Experimental results

In order to verify the validity of the theoretical investigation of Section 3 on the configuration discussed in this paper, an experimental machine was built and tested using the standard frame DZ112M, of a four-pole, 50 Hz, three-phase, 36-stator slot induction motor. The stator winding was rewound to accommodate two sets full pitch, single-layer stator windings, each having the same number of turns per pole per phase. The auxiliary winding was, however, wound using thinner diameter of wire so that the stator slot will accommodate the two sets of windings. The salient pole rotor was milled from the corresponding three-phase squirrel cage induction rotor, such that the ratio of the pole arc to pole pitch is 0.5. The main winding of the machine is supplied directly from the mains utility supply. A simplified block diagram and pictorial representation of the test set-up is shown in Fig. 11. It consists basically of a balanced three-phase supply, a variable dc power source, data acquisition devices, synchronous reluctance machine adapted from an induction machine and a DC machine operated both in the motor mode to synchronise the machine and in the generator to load the synchronous reluctance machine.

Experimental trace of both the main and auxiliary winding voltage and current under no load condition, and with a per phase capacitance value of 60 μF is shown in Fig. 12. The leading current flowing in the auxiliary winding is shown in Fig. 12*b*, and its influence on the main winding current is also seen in Fig. 12*a*. The presence of harmonic is evident

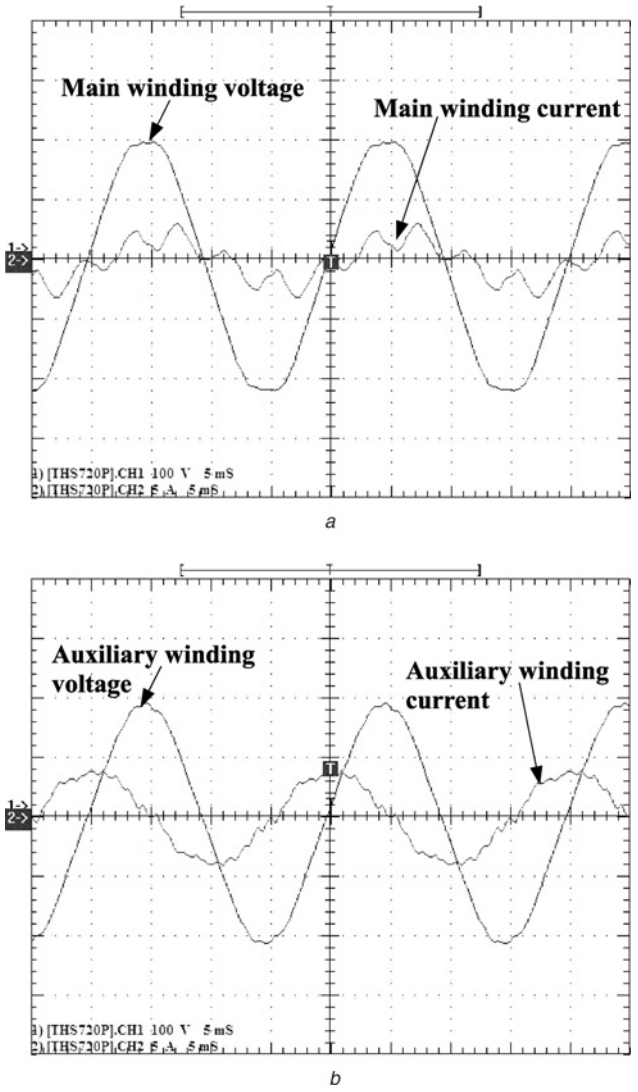

Figure 12 *Experimental trace*

a Main winding
b Auxiliary winding current and voltage with a per phase capacitance of 60 μF

in these trace plots; however, the measured harmonic characteristic of the main winding current of the machine fitted with the configuration discussed in this paper was found to be lower than that of the conventional machine, particularly under load condition.

To compare the variation of the performance characteristics of the motor with auxiliary winding attached to a capacitor, effective reactances X_d' and X_q' of the experimental machine were measured, respectively, using the no-load test and pull out torque tests as described by Honsinger [2, 27]. Before the machine was modified to the new structure, X_d and X_q were, respectively, obtained for the operational voltage of 150 V as 43.41 and 12.60 Ω, thus an unsaturated saliency ratio of 3.44. Additional parameters of the experimental machine are listed in Table 1. In order to experimentally investigate the effect of the new structure discussed in this paper on these critical

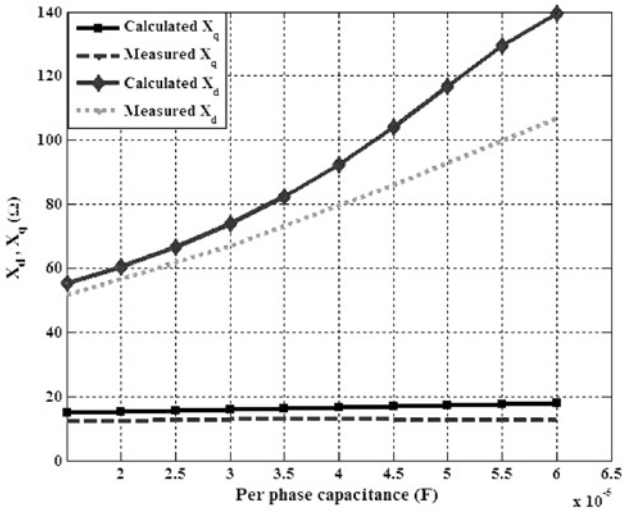

Figure 13 *Calculated and measured effective X_d, X_q as a function of capacitance*

parameters of the machine, balanced capacitors were attached to the auxiliary winding and the effective *d*- and *q*-axis reactances were similarly determined. A graphical representation of the variation of the measured and calculated X_d, X_q and the effective reactance ratio (X_d/X_q) with the size of capacitance are shown in Figs. 13 and 14. It is observed from these figures that the experimental as well as the calculated values generally follow the same trend. The value of effective direct axis reactance X_d as determined from the source obviously increased with the size of the capacitance injected, while that of the quadrature axis reactance was only slightly changed. This result summarily leads to an increase in the effective reactance ratio of the machine. This will likewise improve the stability characteristics of this machine since the

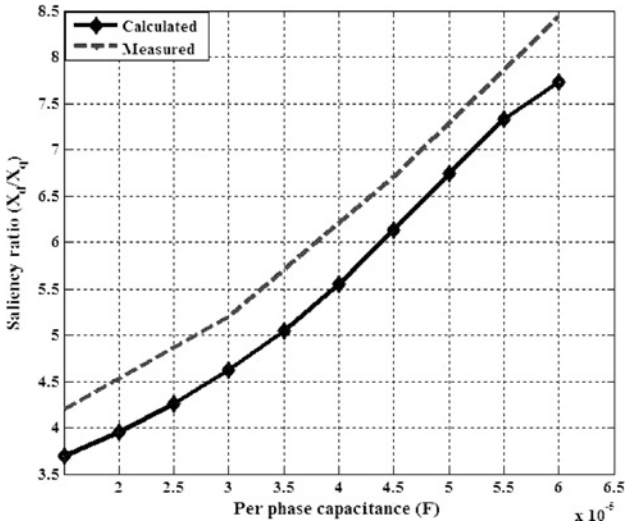

Figure 14 *Calculated and measured effective saliency ratio (X_d/X_q)*

IET Electr. Power Appl., 2010, Vol. 4, Iss. 4, pp. 291–303
doi: 10.1049/iet-epa.2009.0134

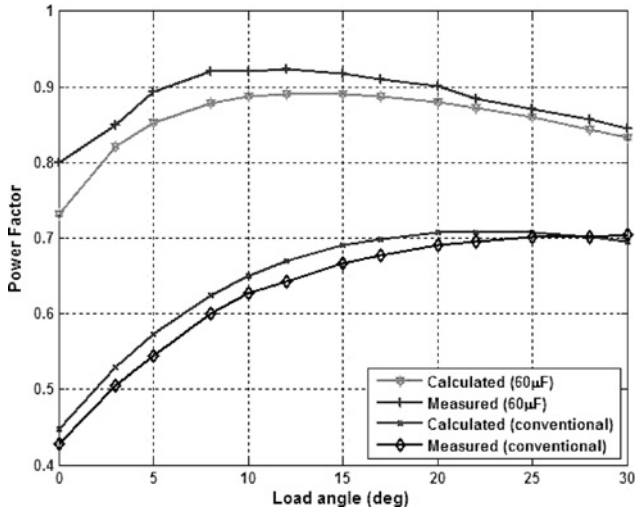

Figure 15 *Measured and calculated power factor*

effective X_d was obviously improved with only a little change to X_q. It has been variously reported and it is well known that a direct increase in the effective reactance ratio of synchronous reluctance machine leads to an improved performance characteristics of a synchronous reluctance machine, therefore this arrangement has successfully improved the power factor and the torque per ampere performance characteristics of a synchronous reluctance machine with a simple salient rotor structure.

Fig. 15 shows a comparative display of the calculated and measured power factor for the conventional machine as well as the machine fitted with a 60 μF capacitor. The improvement of the power factor over the range of operational load angles is evident with this curve, and the power factor of the machine is found to improve with increase in load torque.

To elucidate further, the trade-off between the benefits and cost of the proposed scheme, further experiments were carried out and reported here. Specifically, comparative experimental results of the power factor, torque and efficiency are shown in Table 2 for a 75 μF capacitor attached to the auxiliary winding. Experimental results illustrating the variation of the main winding current, auxiliary winding current and efficiency as a function of the load are as shown in Fig. 16. Although the conventional machine gave a best power factor of 0.70, the machine fitted with the configuration gave a best of about 0.97. The main winding current for both machines expectedly increase with load torque, whereas the measured auxiliary winding current is not influenced by the size of the load, thus it remains relatively constant over the range of operating power. At about 1.2 p.u loading, the conventional machine pulled out of synchronism with much vibration, whereas the machine fitted with the configuration discussed in this paper was able to sustain the loading without oscillation or vibration.

Table 2 also reveals a 134% improvement in power factor at no load and 37% power factor improvement at full load. The torque per ampere of the synchronous reluctance machine is improved by 10.9% at full load without varying the axial length or the volume of the machine. However, the efficiency of the machine marginally decreased by 4.4% at full load. This marginal decrease in efficiency can be effectively minimised with a proper design of the rotor for its stator.

Table 2 Comparative performance characteristics at various loads

Load (pu)	Power factor conventional machine	Power factor machine with 75 μF	% Power factor improvement	Torque/ ampere conventional machine	Torque/ ampere machine with 75 μF	% Torque/ ampere improvement	Efficiency conventional machine	Efficiency machine with 75 F	% Efficiency drop
0.1	0.410	0.957	133.724	0.222	0.421	90.027	0.166	0.127	−23.476
0.2	0.478	0.963	101.696	0.405	0.664	64.007	0.241	0.216	−10.415
0.3	0.536	0.967	80.395	0.573	0.876	52.739	0.310	0.286	−7.777
0.4	0.585	0.969	65.573	0.727	1.056	45.281	0.371	0.340	−8.540
0.5	0.625	0.969	55.031	0.866	1.205	39.221	0.424	0.380	−10.314
0.6	0.656	0.967	47.536	0.990	1.323	33.700	0.466	0.410	−11.991
0.7	0.677	0.963	42.365	1.099	1.410	28.313	0.498	0.433	−12.884
0.8	0.688	0.957	39.093	1.193	1.466	22.821	0.516	0.452	−12.413
0.9	0.690	0.949	37.491	1.273	1.490	17.057	0.522	0.470	−9.910
1.0	0.683	0.939	37.476	1.338	1.483	10.878	0.512	0.490	−4.432
1.2	Pull out	0.927		Pull out	1.445		Pull out	0.514	

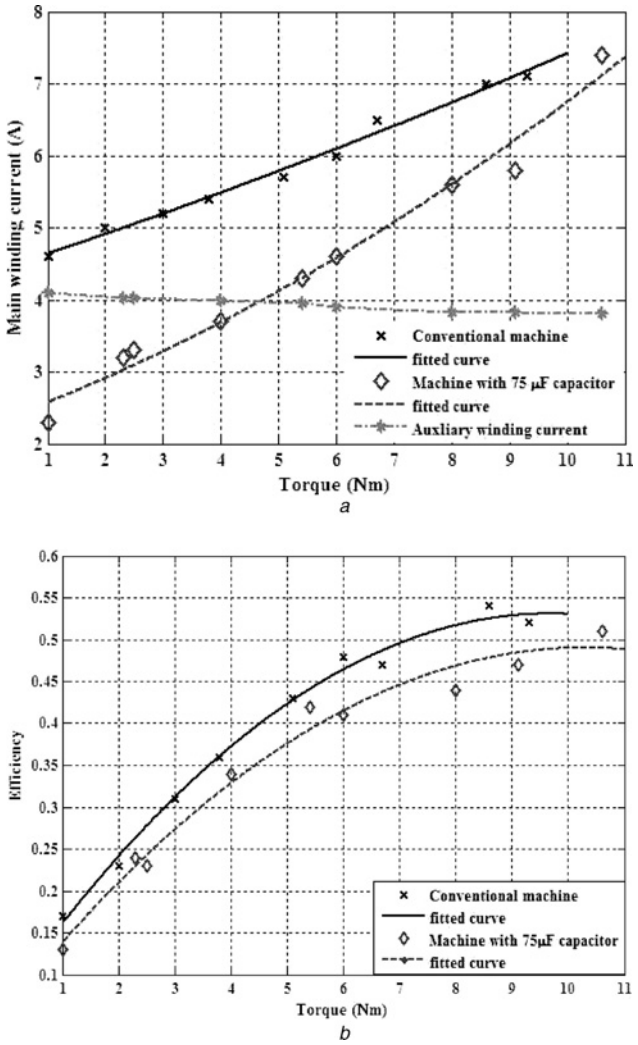

Figure 16 *Measured main winding current and efficiency as a function of torque*

a Variation of the measured main winding current with torque
b Variation of the efficiency with the measured torque

6 Conclusion

A configuration utilising an auxiliary winding connected to a balanced capacitance, to improve the performance characteristics of synchronous reluctance machine with simple salient rotor structure is investigated in this paper. The analysis followed the coupled circuit and the simplified electromagnetic field concepts to provide insight into flux distribution as well as the torque performance of the machine.

Analysis of the machine showed that the net flux in the airgap is sinusoidal, but with a clear presence of third harmonic components.

Following the coupled circuit approach via the impedance evaluation, a suitable size of capacitor that makes the machine to run at a comparatively better power factor was determined, and with this capacitance value, a theoretically high effective reactance ratio was evaluated. The *d*-axis reactance of the machine was boosted whereas the *q*-axis reactance remained fairly constant as against the conventional story of reducing X_q.

Our experimental results on a practical motor validated the analytical results, and clearly demonstrated that the real power factor of the motor can be greatly improved using the configuration discussed in this paper when compared with the conventional reluctance motor. Also, the torque per ampere of the machine is likewise improved (as shown in Table 2) without changing the axial length/volume of the machine. This is made possible by the presence of the auxiliary winding and capacitor which improved the effective reactance ratio of the machine.

With the known advantages and application areas of synchronous reluctance machine with simple salient rotor, the machine fitted with this configuration should find acceptability because of its benefits.

Although the configuration has been applied in this work to a simple salient rotor, consideration has been given to its use in further improving the performance possibilities of other rotor structures such as flux barrier and axially laminated rotor.

7 References

[1] BOLDEA I., FU X., NASAR S.: 'Performance evaluation of axially laminated anisotropic (ALA) rotor reluctance synchronous motors', *IEEE Trans. Ind. Appl.*, 1994, **30**, (4), pp. 977–985

[2] HONSINGER V.: 'Steady state performance of reluctance machines', *IEEE Trans. Power Appar.Syst.*, 1971, **PAS-90**, (1), pp. 304–317

[3] LIPO T.: 'Novel reluctance concepts for variable speed drives'. 'Mediterranean Electrotechnical Conf.', 1991, MELECON, pp. 34–43

[4] TOLIYAT H.A., XU L., LIPO T.A.: 'A five-phase reluctance motor with high specific torque', *IEEE Trans. Ind. Appl.*, 1992, **28**, (3), pp. 659–667

[5] RAKGATI E., KAMPER M.: 'Torque performance of optimally designed three-and five-phase reluctance synchronous machines with two rotor structures', *SAIEEE*, 2006, **97**, (1), pp. 43–49

[6] LIPO T.: 'Synchronous reluctance machines – a viable alternative for ac drives?', *Electr. Mach. Power Syst.*, 1991, **19**, (6), pp. 659–671

[7] VAGATI A.: 'The synchronous reluctance solution: a new alternative in ac drives'. Twentieth Int. Conf. Industrial Electronics, Control and Instrumentations, IECON'94, 1994, pp. 1–12

doi: 10.1049/iet-epa.2009.0134

[8] COATES C.E., PLATT D., GOSBELL V.J.: 'Performance evaluation of a nine-phase synchronous reluctance drive'. Thirty-sixth IAS Annual Meeting, Conference Record of the IEEE Industry Applications, 2001, vol. 3, pp. 2041–2047

[9] MATSUO T., LIPO T.A.: 'Rotor design optimization of synchronous reluctance machine', *IEEE Trans. Energy Convers.*, 1994, **9**, (2), pp. 359–365

[10] TOLIYAT H.A., WAIKAR S.P., LIPO T.A.: 'Analysis and simulation of five phase synchronous reluctance machines including third harmonic of airgap MMF', *IEEE Trans. Ind. Appl.*, 1998, **34**, (2), pp. 332–339

[11] XU L., FU W.N.: 'Evaluation of 3rd harmonic component effects in a 5-phase synchronous reluctance motor drive using time stepping finite element method', *IEEE Trans. Ind. Appl.*, 2002, **38**, pp. 638–644

[12] MULJADI E., LIPO T.A., NOVOTNY D.W.: 'Power factor enhancement of induction machines by means of solid state excitation', *IEEE Trans. Power Electron.*, 1989, **4**, (4), pp. 409–418

[13] AGU L.A., ANIH L.U., OJO O., *ET AL.*: 'Novel synchronous reluctance machine with capacitance injection'. LMH Rotating Machine, Pilansberg Conference Centre, South Africa, 2005, pp. 1–8

[14] WANLASS C.L.: 'US Patent 41887457, 1980

[15] UMANS S.D., HESS H.L.: 'Modelling and analysis of a the Wanlass three-phase induction motor configuration', *IEEE Trans. Power Appar. Syst.*, 1983, **102**, (9), pp. 2912–2916

[16] ROBERTS G.D.: 'US Patent 4808868, 1989

[17] MEDARAMETLA J.B., COX M.D., BAGHZOUZ Y.: 'Calculations and measurement of unity plus three-phase induction motor', *IEEE Trans. Energy Convers.*, 1992, **7**, (4), pp. 732–738

[18] OGUNJUYIGBE A.S.O., JIMOH A.A., NICOLAE D.V.: 'Improving synchronous reluctance machine performance by direct capacitance injection through an auxiliary winding'. ICEMS'07, 2007, pp. 1055–1060

[19] OBE E., SENJYU T.: 'Analysis of a polyphase synchronous reluctance machine with two identical windings', *Electr. Power Syst. Res.*, 2006, **76**, pp. 515–524

[20] SCHRIFERL R., ONG C.: 'Six phase synchronous machine with ac and dc stator connections, part 1:Equivalent circuit representations and steady state analysis', *IEEE Trans. Power Appar. Syst.*, 1983, **PAS-102**, pp. 2685–2693

[21] FUCHS E., ROSENBURG L.: 'Analysis of alternator with two displaced windings', *IEEE Trans. Power Appar. Syst.*, 1974, **PAS-93**, pp. 1776–1786

[22] TOUMA-HOLMBERG M., STRIVASTA K.: 'Double winding, high voltage cable wound generator: Steady state and fault analysis', *IEEE Trans. Energy Convers.*, 2004, **19**, pp. 245–250

[23] HENDERSPORT J.R., MILLER T.J.E., STATON D.A.: 'The synchronous reluctance motor for motion control applications', http://www.jimhendershot.com/synchronous%20reluctance%20motor%20for%20motion%20control%20applications.pdf, accessed: 13/12/2008

[24] SPOONER E., WILLIAMS A.: 'Mixed pole windings and some applications', *IEE Proc.*, 1990, **137**, (pt. B), pp. 89–97

[25] KRAUSE P.: 'Analysis of electric machinery' (McGraw-Hill Book Company, 1986)

[26] OJO O., DONG G., OMOIGUI M.: 'Analysis of a synchronous reluctance machine with an auxiliary single phase winding', *IEEE Trans. Ind. Appl.*, 2003, **39**, pp. 1307–1313

[27] HONSINGER V.: 'The inductances Ld and Lq of reluctance machines', *IEEE Trans. Power Appar. Syst.*, 1971, **PAS-90**, pp. 298–304

8 Appendix

$$Z_{\mathrm{T-ph}} = (r_{s1} + \mathrm{j}X_{L1}) + \left[\frac{\mathrm{j}X_{\mathrm{m}}(r_{s2} + \mathrm{j}(X_{L2} - X_{\mathrm{c}}))}{\mathrm{j}X_{\mathrm{m}} + r_{s2} + \mathrm{j}(X_{L2} - X_{\mathrm{c}}))}\right] \quad (20)$$

When (20) is expanded, the imaginary part of the total impedance is obtained as

$$\mathrm{Imag}(Z_{\mathrm{T-ph}}) = \frac{(r_{s2}^2 + (X_{L2} - X_{\mathrm{c}} + X_{\mathrm{m}}))X_{L1} + X_{\mathrm{m}}r_{s2}^2 - X_{\mathrm{m}}(X_{L2} - X_{\mathrm{C}})(X_{\mathrm{m}} + X_{L2} - X_{\mathrm{C}})}{r_{s2}^2 + (X_{L2} - X_{\mathrm{c}} + X_{\mathrm{m}})^2} \quad (21)$$

If we set (21) to zero, we have

$$\mathrm{Imag}(Z_{\mathrm{T-ph}}) = X_{\mathrm{C}}^2(X_{L1} - X_{\mathrm{m}}) - X_{\mathrm{C}}(2X_{L1}X_{\mathrm{m}} + 2X_{L1}X_{L2} - X_{\mathrm{m}}^2) + r_{s2}^2X_{L1} + 2X_{L1}X_{L2}X_{\mathrm{m}} + X_{L1}X_{L2}^2 + X_{L1}X_{\mathrm{m}}^2 + X_{\mathrm{m}}r_{s2}^2 - X_{L2}X_{\mathrm{m}}^2 - X_{\mathrm{m}}X_{L2}^2 \quad (22)$$

This equation can be compared to a quadratic equation of the form

$$aX_{\mathrm{C}}^2 + bX_{\mathrm{C}} + C = 0 \quad (23)$$

which gives a solution

$$X_{\mathrm{C}} = \frac{-b \pm \sqrt{b^2 - 4ac}}{2a} \quad (24)$$

The quadratic solution gives the two capacitance value X_{C1} and X_{C2}.